

Scalar dark matter in the conformally invariant extension of the standard model

Dong-Won Jung,^{*} Jungil Lee,[†] and Soo-hyeon Nam[‡]

Department of Physics, Korea University, Seoul 02841, Korea

(Dated: May 3, 2022)

We study a classically scale-invariant model with an electroweak singlet scalar mediator together with a scalar dark matter multiplet of global $O(N)$ symmetry. Our most general conformally invariant scalar potential generates the electroweak symmetry breaking via the Coleman-Weinberg mechanism, and the new scalar singlet acquires its mass through radiative corrections of the SM particles and the scalar dark matter. Taking into account the collider bounds, we present the allowed region of new physics parameters satisfying the recent measurement of relic abundance. With the obtained parameter sets, we predict the elastic scattering cross section of the new scalar multiplet into target nuclei for a direct detection of the dark matter. We also perform a full analysis with arbitrary set of parameters for $N \geq 2$, and discuss the implication of the constraints from the on-going direct and indirect detections of dark matter.

^{*} dongwonj@korea.ac.kr

[†] jungil@korea.ac.kr

[‡] glvnsh@gmail.com

I. INTRODUCTION

Since the discovery of the Higgs boson at the Large Hadron Collider (LHC) [1, 2], the Standard Model (SM) has been remaining quite successful in spite of many experimental pursuits of physics beyond the SM (BSM). Nevertheless, the story has not been completed yet: Higgs self coupling λ_h should be measured to prove or disprove whether the Higgs mechanism is the root cause of the Electroweak Symmetry Breaking (EWSB) or not. Besides this lack of the experimental confirmation of the EWSB mechanism, there are still many open questions both theoretically and phenomenologically. Among them are the gauge hierarchy problem that addresses the smallness of the EWSB scale compared to the Planck scale M_P , and non-baryonic dark matter (DM) of the Universe.

In 1995, Bardeen [3] suggested that softly broken conformal (scale) invariance could be a possible solution for the hierarchy problem. If conformal invariance is assumed at classical level, there is no dimensionful parameter in the Lagrangian and conformal symmetry is broken only logarithmically through the conformal anomaly with dimension-4 operators at quantum level. Many works have been done along this line with the EWSB by dimensional transmutation [4–22], or radiative mechanisms [23–74] of Coleman-Weinberg (CW) [75] types. In many of those works, the DM models are embedded at the same time. Incorporating the DM in a conformally invariant setup is highly motivated since in both cases BSM particles are required. For example, a naive Coleman-Weinberg type of the model suffers instability arising from radiative corrections because of the large top-quark mass, so it should be stabilized with the introduction of additional bosonic degrees of freedom. As one of the simplest extensions of the SM, one can introduce a gauge-singlet Higgs-portal scalar DM, and make it stabilize the Higgs mass via the CW mechanism as shown in Refs. [56, 57]. However, generating a proper Higgs mass requires a large enough mass of the scalar DM, so that the Higgs-scalar couplings become too large. As a result, this kind of a simple setup makes the theory non-perturbative at a few TeV scale, which is undesirable. This issue can be resolved by separating the new scalar responsible for the EWSB from the DM sector.

In this work, we propose the conformally invariant DM model which contains an $SU(2)$ doublet Higgs field, a scalar mediator together with hidden sector scalar particles with $O(N)$ global symmetry for the stability of the hidden sector. With the most general conformally invariant Lagrangian, we employ the framework of Gildener-Weinberg (GW) [76], where a flat direction at tree-level is lifted by radiative corrections. In this way, the vacuum structure is determined and a light pseudo Nambu-Goldstone boson, called ‘scalons’, appears as a result of conformal symmetry breaking. Through its mixing with the SM-like Higgs boson, two light scalar particles emerge in the model that interact with both visible and hidden sectors. In particular, there exist contact interactions of the DMs and, as a result, the model takes the form of so-called the ‘secluded’ DM [77] scenarios as a conformally invariant version.

This paper is organized as follows. In Sec. II, we describe the model in detail including the determination of the flat direction in a similar manner to the GW framework. Next, the effective potential obtained by the CW mechanism and the radiatively induced scalar masses are presented at one-loop level in Sec. III. In Sec. IV, we provide a detailed phenomenological analysis of the DM physics such as the relic density and the direct detection. Section V is devoted to a summary and the conclusion.

II. MODEL

We consider a dark sector consisting of two classically massless real scalar fields S and ϕ , which are SM gauge singlets. The scalar mediator S is responsible for the EWSB together with the SM Higgs doublet H , and the scalar ϕ is a DM candidate chosen to be the fundamental representation of a global $O(N)$ group, $\phi = (\phi_1, \dots, \phi_N)^T$. The extended Higgs sector Lagrangian with the renormalizable DM interactions is then given by

$$\mathcal{L}_{\text{DM}} = (D_\mu H)^\dagger D^\mu H + \frac{1}{2}(\partial^\mu S)^2 + \frac{1}{2}(\partial_\mu \phi^T)\partial^\mu \phi - V(H, S, \phi), \quad (1)$$

where the scale-invariant scalar potential is

$$V(H, S, \phi) = \lambda_h(H^\dagger H)^2 + \frac{1}{2}\lambda_{hs}H^\dagger HS^2 + \frac{1}{2}\lambda_{h\phi}H^\dagger H\phi^T\phi + \frac{1}{4}\lambda_{s\phi}S^2\phi^T\phi + \frac{1}{4}\lambda_s S^4 + \frac{1}{4}\lambda_\phi(\phi^T\phi)^2. \quad (2)$$

A similar model was studied recently for $N = 2$ case in Refs. [64, 73], but they simply assumed $\lambda_{h\phi} = 0$ in order to decouple the DM sector from the SM Higgs. In general, however, such an interaction term is not forbidden by a discrete symmetry such as Z_2 symmetry theoretically, and also it is very important to explain the current astronomical observables phenomenologically, as we will show in Sec. V.

After the EWSB, the DM scalar ϕ takes a vanishing VEV while the neutral component of the SM Higgs and the singlet scalar S develop nonzero VEVs, $\langle H^0 \rangle = v_h/\sqrt{2}$ and $\langle S \rangle = v_s$, respectively. Adopting the GW approach, we

choose a flat direction among the scalar VEVs along which the potential in Eq. (2) vanishes at some scale $\mu = \Lambda$. Along that flat direction, the potential minimization conditions $\partial V/\partial H|_{\langle H^0 \rangle = v_h/\sqrt{2}} = \partial V/\partial S|_{\langle S \rangle = v_s} = 0$ lead to the following relations

$$\lambda_{hs}(\Lambda) = -2\lambda_h(\Lambda)/t_\beta^2, \quad \lambda_s(\Lambda) = \lambda_h(\Lambda)/t_\beta^4, \quad (3)$$

where $t_\beta (\equiv \tan \beta) = v_s/v_h$. The neutral scalar fields h and s defined by $H^0 = (v_h + h)/\sqrt{2}$ and $S = v_s + s$ are mixed to yield the mass matrix:

$$\mu_h^2 = 2\lambda_h v_h^2, \quad \mu_s^2 = 2\lambda_h v_h^2/t_\beta^2, \quad \mu_{hs}^2 = -2\lambda_h v_h^2/t_\beta. \quad (4)$$

The corresponding scalar mass eigenstates h_1 and h_2 are admixtures of h and s :

$$\begin{pmatrix} h_1 \\ h_2 \end{pmatrix} = \begin{pmatrix} \cos \theta & -\sin \theta \\ \sin \theta & \cos \theta \end{pmatrix} \begin{pmatrix} h \\ s \end{pmatrix}, \quad (5)$$

where the mixing angle θ is given by

$$\tan \theta = \frac{y}{1 + \sqrt{1 + y^2}}, \quad y \equiv \frac{-2\mu_{hs}^2}{\mu_h^2 - \mu_s^2}. \quad (6)$$

Combining Eqs. (4) and (6), we have $\tan \theta = -t_\beta$ or $1/t_\beta$. The mixing angle θ is expected to be very small (less than about 0.2) due to the LEP constraints. If $\tan \theta = -t_\beta$, then $\lambda_s = \lambda_h/\tan^4 \theta$ from Eq. (3) so that λ_s becomes very large. But this case is theoretically disfavored because of the failure of the perturbativity of the couplings. Also, experimental constraints disfavor this scenario as well [40]. Therefore, we only consider the case of $\tan \theta (\equiv t_\theta) = 1/t_\beta$, which results in $\sin \theta (\equiv s_\theta) = c_\beta$ and $\cos \theta (\equiv c_\theta) = s_\beta$. In this case, λ_{hs} and λ_s are suppressed by t_θ^2 and t_θ^4 , respectively, which ensures the perturbativity of those couplings and induces the suppression of the Higgs portal interactions.

After diagonalizing the mass matrix, we obtain the physical masses of the two scalar bosons (h_1, h_2) and the DM scalar ϕ as follows:

$$M_1^2 = 2\lambda_h v^2 t_\theta^2, \quad M_2^2 = 0, \quad M_\phi^2 = \frac{v^2}{2} (\lambda_{h\phi} s_\theta^2 + \lambda_{s\phi} c_\theta^2), \quad (7)$$

where $v \equiv \sqrt{v_h^2 + v_s^2}$. We assume that M_1 corresponds to the observed SM-like Higgs boson mass in what follows. The SM Higgs h_1 and the DM scalars ϕ have the tree-level masses while the new scalar singlet h_2 acquires its mass through radiative corrections, which is similar to the cases considered in Refs. [50, 64]. In terms of the physical states, the tree-level scalar potential in the flat direction can be expressed in the unitary gauge as

$$\begin{aligned} V(h_1, h_2, \phi_i) = & \frac{1}{2} M_1^2 h_1^2 + \frac{1}{2} M_\phi^2 \phi_i^2 + \frac{\lambda_h}{4} \left[(1 - t_\theta^2)^2 h_1^4 + 4t_\theta(1 - t_\theta^2) h_1^3(h_2 + v) + 4t_\theta^2 h_1^2(h_2^2 + 2vh_2) \right] \\ & + \frac{1}{4} \left[(c_\theta^2 \lambda_{h\phi} + s_\theta^2 \lambda_{s\phi}) h_1^2 + (s_\theta^2 \lambda_{h\phi} + c_\theta^2 \lambda_{s\phi}) (h_2^2 + 2vh_2) + s_{2\theta} (\lambda_{h\phi} - \lambda_{s\phi}) h_1(h_2 + v) \right] \phi_i^2 + \frac{1}{4} \lambda_\phi (\phi_i^2)^2, \end{aligned} \quad (8)$$

where $s_{2\theta} \equiv \sin 2\theta$. Note that we have discarded some of the scalar interaction terms in the potential in Eq. (8) by imposing the constraints in Eq. (3). For instance, the $h_1 h_2^2$ interaction is absent because the relevant Higgs-scalar coupling $c_{122} \propto 1 - t_\beta t_\theta$ vanishes under the constraint $t_\theta = 1/t_\beta$. Therefore, even if the radiatively generated h_2 mass is less than a half of the h_1 mass, the partial decay width $\Gamma(h_1 \rightarrow h_2 h_2)$ is negligible and our model is not constrained by the invisible Higgs decay measurements.

III. EFFECTIVE POTENTIAL

The original approach of GW expressed the one-loop effective potential in terms of the spherical-coordinate (radial) field of the scalar gauge eigenstates. Rather differently, we derive the effective potential with the physical eigenstates of the scalars and obtain the scalar masses at one-loop level directly. Let the background value of the physical scalar h_i be h_{ic} . Then the effective potential is obtained by expanding the interaction terms in the Lagrangian around the background fields h_{ic} and by keeping terms quadratic in fluctuating fields only. From Eq. (8), the effective potential at one-loop level is given by

$$V_{\text{eff}}(h_{1c}, h_{2c}) = V^{(0)}(h_{1c}, h_{2c}) + V^{(1)}(h_{1c}, h_{2c}), \quad (9)$$

with

$$V^{(0)}(h_{1c}, h_{2c}) = \frac{\lambda_h}{4} \left[(1 - t_\theta^2)^2 h_{1c}^4 - 4t_\theta(1 - t_\theta^2) h_{1c}^3 h_{2c} + 4t_\theta^2 h_{1c}^2 h_{2c}^2 \right],$$

$$V^{(1)}(h_{1c}, h_{2c}) = \sum_P n_P \frac{\bar{m}_P^4(h_{ic})}{64\pi^2} \left(\ln \frac{\bar{m}_P^2(h_{ic})}{\mu^2} - c_P \right), \quad (10)$$

where $c_P = 3/2$ ($5/6$) for scalars and fermions (gauge bosons) in the $\overline{\text{MS}}$ scheme and μ is a renormalization scale. \bar{m}_P is a field-dependent mass and the summation is over the particle species of fluctuating fields $P = h_{1,2}, Z, W^\pm, t, \phi_i$ and their degrees of freedoms (n_P) are given as follows

$$n_{h_1} = n_{h_2} = n_{\phi_i} = 1, \quad n_Z = 3, \quad n_{W^\pm} = 6, \quad n_t = -12. \quad (11)$$

Taking the flat direction of the VEVs, we minimize the effective potential at $h_{1c} = 0$ and $h_{2c} = v$, which corresponds to $h_c = v_h$ and $s_c = v_s$ in terms of the background values of the scalar gauge eigenstates. The field-dependent mass $\bar{m}_P(h_{ic})$ is proportional to h_{ic} , so that $\bar{m}_P(h_{1c})$ is irrelevant to our study because $\partial \bar{m}_P(h_{1c}) / \partial h_{1c}|_{h_{1c}=0} = 0$. The relevant field-dependent masses for h_{2c} are obtained as

$$\bar{m}_{h_1}^2(h_{2c}) = 2\lambda_h t_\theta^2 h_{2c}^2, \quad \bar{m}_{h_2}^2(h_{2c}) = 0, \quad \bar{m}_{\phi_i}^2(h_{2c}) = \frac{1}{2} (\lambda_{h\phi} s_\theta^2 + \lambda_{s\phi} c_\theta^2) h_{2c}^2,$$

$$\bar{m}_Z^2(h_{2c}) = M_Z^2 \frac{h_{2c}^2}{v^2}, \quad \bar{m}_{W^\pm}^2(h_{2c}) = M_W^2 \frac{h_{2c}^2}{v^2}, \quad \bar{m}_t^2(h_{2c}) = M_t^2 \frac{h_{2c}^2}{v^2}. \quad (12)$$

The masses of the physical scalars h_i can be directly obtained by taking the second-order derivatives of the effective potential with respect to the classical background fields h_{ic} as

$$M_1^2 = \frac{\partial^2 V_{\text{eff}}}{\partial h_{1c}^2} \Big|_{h_{1c}=0, h_{2c}=v} = 2\lambda_h v^2 t_\theta^2,$$

$$M_2^2 = \frac{\partial^2 V_{\text{eff}}}{\partial h_{2c}^2} \Big|_{h_{1c}=0, h_{2c}=v} = \frac{1}{8\pi^2 v^2} (M_1^4 + 6M_W^4 + 3M_Z^4 - 12M_t^4 + NM_\phi^4). \quad (13)$$

Although we have employed the strategy somewhat different from those of earlier studies following the GW approach in Refs. [50, 64], the final results for the scalar masses are equivalent. One can read off the inequality $NM_\phi^4 \geq 12M_t^4 - M_1^4 - 6M_W^4 - 3M_Z^4$ from Eq. (13) and find that $M_\phi \gtrsim 265$ GeV for $N = 2$. In total, besides N , we have five independent model parameters relevant to DM phenomenology. The four model parameters λ_h , v_s , $\lambda_{h\phi}$, and $\lambda_{s\phi}$ determine the masses $M_{1,2}$, M_ϕ , and the mixing angle θ , while the DM self coupling λ_ϕ is irrelevant to our study on the DM-SM interactions. The dependency of the model parameters are

$$v = \frac{v_h}{s_\theta}, \quad v_s = \frac{v_h}{t_\theta}, \quad \lambda_h = \frac{M_1^2 c_\theta^2}{2v_h^2}, \quad \lambda_{hs} = -\frac{M_1^2 s_\theta^2}{v_h^2}, \quad \lambda_s = \frac{M_1^2 s_\theta^2 t_\theta^2}{2v_h^2}, \quad \lambda_{s\phi} = \left(\frac{2M_\phi^2}{v_h^2} - \lambda_{h\phi} \right) t_\theta^2. \quad (14)$$

Given the fixed Higgs mass M_1 and $v_h \simeq 246$ GeV, we constrain three independent new physics (NP) parameters by taking into account various theoretical considerations and experimental measurements in the next section.

IV. RESULTS OF ANALYSIS

In this section we turn to the phenomenological analysis of the model, especially with the global $O(2)$ symmetry in the hidden sector. It corresponds to the case containing two exact copies of the DM. Using the conditions provided in Sec. III, we perform the numerical analysis by varying the following three NP parameters: t_θ , M_ϕ , $\lambda_{h\phi}$. Let us first consider the relic density. At present, the most accurate determination of the DM mass density Ω_{DM} comes from global fits of cosmological parameters to a variety of observations such as measurements of the anisotropy of the cosmic microwave background (CMB) data by the Planck experiment and of the spatial distribution of galaxies [78]:

$$\Omega_{\text{DM}} h^2 = 0.1186 \pm 0.0020. \quad (15)$$

This relic density observation will exclude some regions in the model parameter space. The relic density analysis in this section includes all possible channels of the $\phi_i \phi_i$ pair annihilation into the SM particles. In this work, we implement the model described in Sec. II into the CalcHEP package [79]. By employing the numerical package `micrOMEGAs` [80]

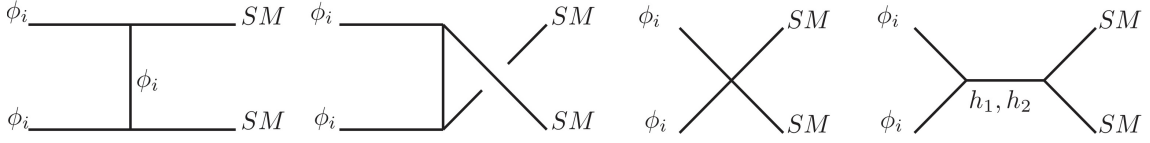


FIG. 1. Relevant Feynman diagrams for relic density calculation.

that includes the CalcHEP for computing the relevant annihilation cross sections, we compute the DM relic density and the spin-independent DM-nucleon scattering cross sections.

The relic density is determined by solving the Boltzmann equation, which contains the thermal average of the cross section times DM velocity v_{DM} as a proportional factor. By expanding this factor in powers of v_{DM} , we find that

$$\langle \sigma v_{\text{DM}} \rangle \propto \frac{1}{4M_\phi^2} \sqrt{1 - \frac{M_{\text{SM}}^2}{M_\phi^2}} |\mathcal{M}|^2 + \mathcal{O}(v_{\text{DM}}^2). \quad (16)$$

The relevant Feynman diagrams are shown in Fig. 1. When the final states are the SM particles other than Higgs-like bosons such as h_1 and h_2 , the only contributions are from the s -channel diagrams exchanging h_1 and h_2 . The amplitude can be expanded in powers of a small parameter M_{SM}^2/M_ϕ^2 :

$$|\mathcal{M}| \sim v_h g_{\text{SM}} \left[\frac{\lambda_{h\phi}}{4M_\phi^2} + \frac{1}{16M_\phi^4} [\lambda_{h\phi} (M_1^2 c_\theta^2 + M_2^2 s_\theta^2) + \lambda_{s\phi} (M_2^2 - M_1^2) c_\theta^2] + \dots \right], \quad (17)$$

where g_{SM} indicates a coupling of h_i and the SM particle interactions. Note that the $\lambda_{s\phi}$ scales as M_ϕ^2 as shown in Eq. (14). Nevertheless, the expression in Eq. (17) demonstrates that the actual contribution of $\lambda_{s\phi}$ to $\langle \sigma v_{\text{DM}} \rangle$ first emerges only at the next-to-leading order in M_{SM}^2/M_ϕ^2 . Thus, both of $\lambda_{h\phi}$ and $\lambda_{s\phi}$ scale similarly, and as a result, those contributions to $\langle \sigma v_{\text{DM}} \rangle$ scale like $\sim 1/M_\phi^6$.

Higgs-like boson pairs such as $h_i h_i$ can be created through various topologies including s -, t -, u -channels, and contact interactions as shown in Fig. 1. This is in contrast to the pure SM final states excluding Higgs-like particles that are created only through the s -channel diagrams. For example, when the final states are a pair of h_1 's, the amplitude at leading order in v_{DM} and M_{SM}^2/M_ϕ^2 is approximately given as

$$|\mathcal{M}| \sim \left| (s \text{ channel}) - v_h^2 c_\theta^2 \frac{(\lambda_{h\phi} - \lambda_{s\phi})^2}{M_\phi^2} + (\lambda_{h\phi} c_\theta^2 + \lambda_{s\phi} s_\theta^2) + \dots \right|. \quad (18)$$

Substituting this $|\mathcal{M}|$ into Eq. (16), we obtain $\langle \sigma v_{\text{DM}} \rangle$. The leading contribution of $\lambda_{h\phi}$ to $\langle \sigma v_{\text{DM}} \rangle$ scales as $1/M_\phi^2$ while that of $\lambda_{s\phi}$ scales as M_ϕ^2 . As a result, as the DM mass increases, the contributions of $\lambda_{h\phi}$ and $\lambda_{s\phi}$ to the relic density vary in opposite directions: the relic density is enhanced by $\lambda_{h\phi}$ -dependent interaction and is reduced by the $\lambda_{s\phi}$ counterpart.

The numerical results for the relic density are shown in Fig. 2. We choose four different values of the mixing angle $t_\theta = 0.05, 0.1, 0.15$, and 0.2 as benchmark points. The left panel of Fig. 2 shows the behavior of the relic density as a function of the DM mass for $\lambda_{h\phi} = 0.01$. At this value of $\lambda_{h\phi}$, the $\lambda_{h\phi}$ contribution is negligible unless t_θ is very small. This generic suppression is originated from the scaling rule $\lambda_{s\phi} \sim t_\theta^2$ given in Eq. (14). Thus, only for $t_\theta = 0.05$ and for the small DM mass, $\lambda_{h\phi}$ contribution can compete with $\lambda_{s\phi}$'s and a local maximum appears. For other values of t_θ , $\lambda_{s\phi}$ contribution dominates and relic density is a decreasing function of the DM mass M_ϕ as shown in the figure. The right panel shows the case of $\lambda_{h\phi} = 0.3$, in which the $\lambda_{h\phi}$ contributions are not negligible at all. In that case, for small values of DM mass, $\lambda_{h\phi}$ contributions are dominant and the relic density is increasing as we increase the DM mass. In the case of large DM masses, $\lambda_{s\phi}$ is enhanced and its contributions make the relic density a decreasing function of the DM mass. Again, the mixing angle suppression of the $\lambda_{s\phi}$ makes the overturn of the relic density take place at larger DM mass when t_θ is smaller. The dotted vertical line represents the minimally allowed DM mass which is determined by the condition of non-tachyonic mass for h_2 , the pseudo Goldstone boson of the spontaneously broken conformal symmetry of the model. If there is an $O(2)$ symmetry in the hidden sector, it means that there exist two exactly the same copies of the DM, and the minimum value of their masses is about ~ 265 GeV.

In Fig. 3, we show the parameter space satisfying the observed relic density in 3σ range for four different values of the mixing angles $t_\theta = 0.05, 0.1, 0.15$ and 0.2 . We have imposed the perturbativity constraints to all of the dimensionless couplings in such a way that they should be smaller than 4π , and the DM mass has been scanned up to 2 TeV. Precise measurements of the relic density result in strong correlations between $\lambda_{h\phi}$ and the DM mass M_ϕ , which is directly

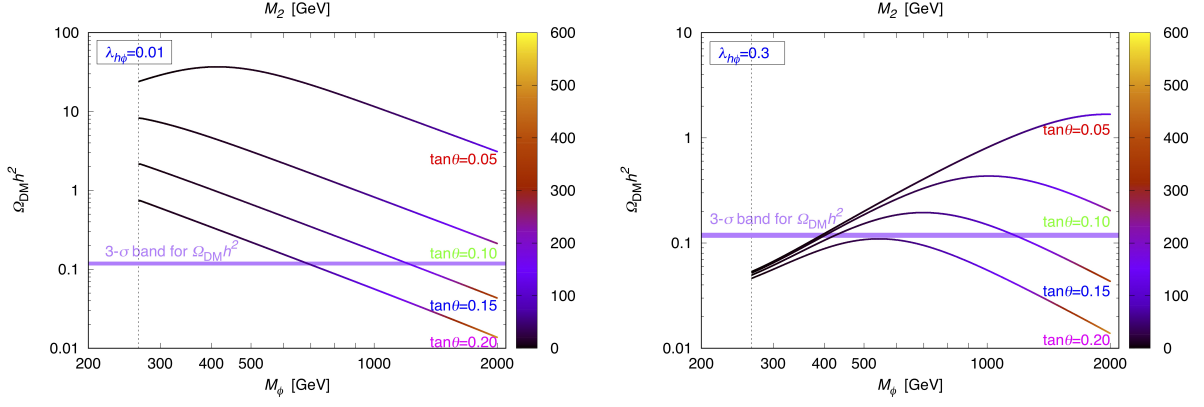


FIG. 2. Relic density Ω_{DM} as a function of the DM mass M_ϕ , for $\lambda_{h\phi} = 0.01$ (left panel) and $\lambda_{h\phi} = 0.3$ (right panel). The vertical dotted line indicates the minimum value of M_ϕ obtained in Eq. (13) for $N = 2$.

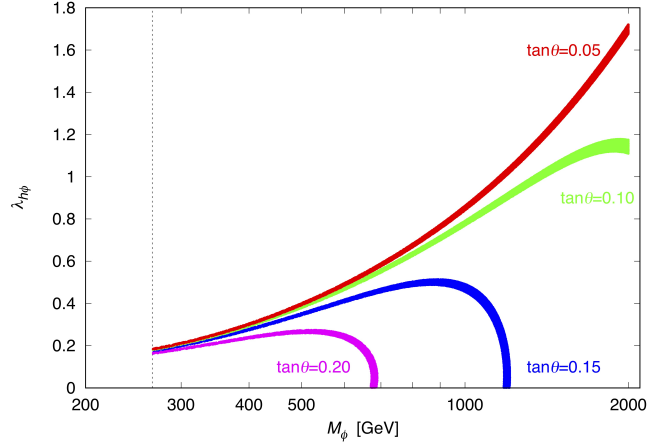


FIG. 3. Allowed regions for the parameter set $(M_\phi, \lambda_{h\phi})$ by relic density observations within 3σ range for four different values of $\tan\theta$. The vertical dotted line indicates the minimum value of M_ϕ obtained in Eq. (13) for $N = 2$.

related to $\lambda_{s\phi}$, depending on the mixing angle t_θ . Since $\lambda_{s\phi}$ has a factor t_θ^2 as addressed in the previous paragraph, it is easy to see that the larger values of $\lambda_{h\phi}$ are disfavored by the observed relic density for large mixing angles. Another interesting point is that there exists an upper bound for the DM mass for the given values of the mixing angle θ .



FIG. 4. Relevant Feynman diagrams for spin-independent DM-nucleon scattering cross section.

Next, let us consider the implications of the direct detection experiments on the model. Non-observation of DM-nucleon scattering events is interpreted as an upper bound on DM-nucleon cross section. The most stringent bound is given by Xenon1T experiment [81] in 2018. Around the same time, LUX [82] and PandaX-II [83] collaborations reported similar but slightly less stringent results. The DM-nucleon scattering occurs only through the two t -channel diagrams exchanging h_1 and h_2 that are shown in Fig. 4. The cross section for this elastic scattering of the highly

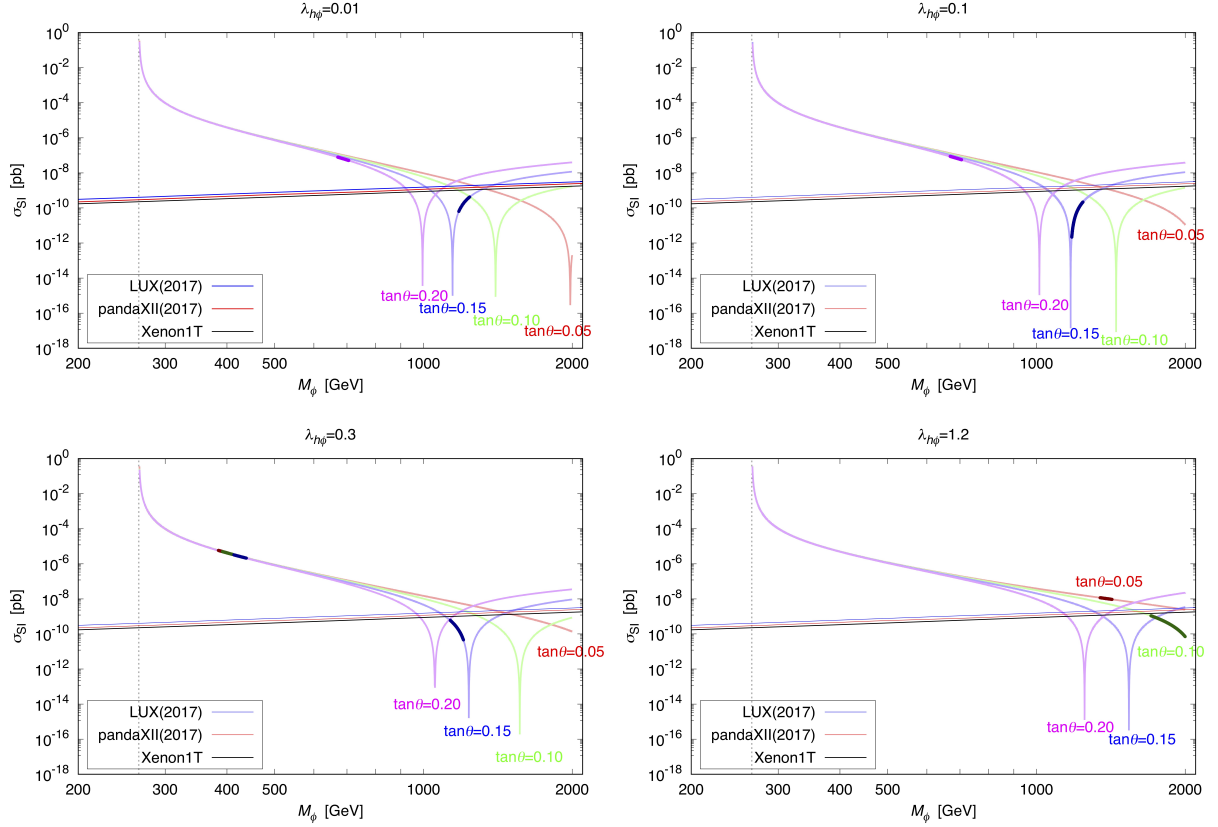


FIG. 5. Spin-independent DM-nucleon scattering cross section as a function of DM mass. The thick bands are allowed by relic density observations, and the vertical dotted line indicates the minimum value of M_ϕ obtained in Eq. (13) for $N = 2$.

non-relativistic DM is well approximated by expanding the amplitude in powers of the velocity v_{DM} of the DM:

$$\sigma \propto \frac{1}{M_\phi^2} |\mathcal{M}|^2, \quad |\mathcal{M}| \sim g_{hNN}^{\text{SM}} v_h \left| \lambda_{h\phi} \left(\frac{s_\theta^2}{M_2^2} + \frac{c_\theta^2}{M_1^2} \right) + \lambda_{s\phi} c_\theta^2 \left(\frac{1}{M_2^2} - \frac{1}{M_1^2} \right) + \dots \right|. \quad (19)$$

In the limit that $\lambda_{h\phi}$ is negligible and $M_2 \approx M_1$, the cross section is severely suppressed because of a strong cancellation between the two t -channel diagrams exchanging h_1 and h_2 . If h_2 becomes very light, then the kinematic enhancement of the h_2 exchange diagram dominates over the contribution of the SM-like Higgs boson h_1 . In addition to that, M_2^2 is proportional to s_θ^2 , and $\lambda_{s\phi}$ to t_θ^2 , the mixing angle dependence disappears in the small DM mass limit. This property is clearly observed in Fig. 5. As we increase the DM mass, $\lambda_{s\phi}$ increases as well and h_1 contributions become more significant. The cross sections hit those minima when $M_2 \simeq M_1$ and increase again mainly due to $\lambda_{s\phi}$. Such a behavior is obviously revealed in the first figure in Fig. 5 where $\lambda_{h\phi} = 0.01$ is small enough to be neglected. When $\lambda_{h\phi}$ is large, a dip appears for slightly heavier h_2 . This manifests itself in Fig. 5 in such a way that the locations of the dip is moved to the right, in the larger DM mass area for larger values of $\lambda_{h\phi}$. The points allowed by the relic density measurement is also presented as thick bands. In Fig. 6, we show the allowed parameter sets of M_ϕ and M_2 over the parameter space,

$$\lambda_{h\phi} \in [0, 4\pi], \quad M_\phi/\text{GeV} \in [265, 2000], \quad t_\theta \in [0, 0.2]. \quad (20)$$

All of the points are consistent with the relic density measurements within 3σ range, and the thick region is allowed by the direct detection measurement bounds. This is our main prediction of the extra scalar mass M_2 and the mixing angle θ , depending on the DM mass M_ϕ . We also provide with a lower bound around ~ 988 GeV for the DM mass M_ϕ , which is valid for all $O(N)$ types of model with $N \geq 2$.

It is straightforward to extend our model to have $O(N)$ symmetry to stabilize the DM in the hidden sector. It corresponds to the case that there exist N copies of the DM with the identical properties except that the minimum value for the DM mass M_ϕ can be lowered according to Eq. (13). The results for the $O(N)$ extension are shown in Fig. 7 for $t_\theta = 0.10$ (left) and 0.15 (right). One can see that a larger value of $\lambda_{h\phi}$ is required for a larger value of N .

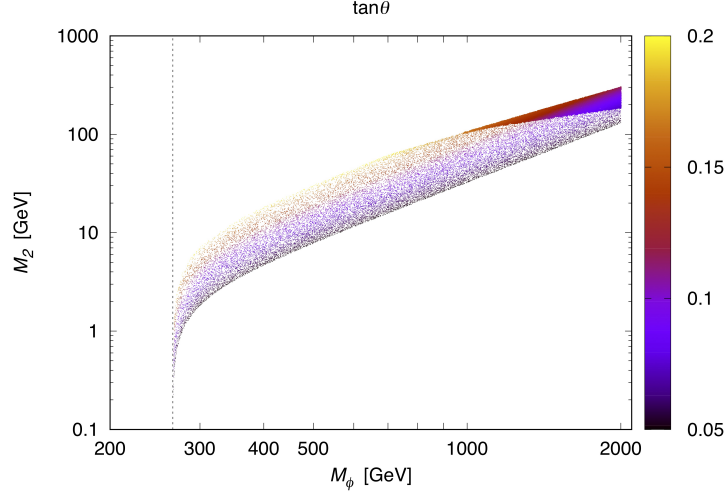


FIG. 6. Allowed parameter sets of (M_ϕ, M_2) by relic density observations in 3σ range. Thick points are allowed by the direct detection bounds as well. The vertical dotted line indicates the minimum value of M_ϕ obtained in Eq. (13) for $N = 2$.

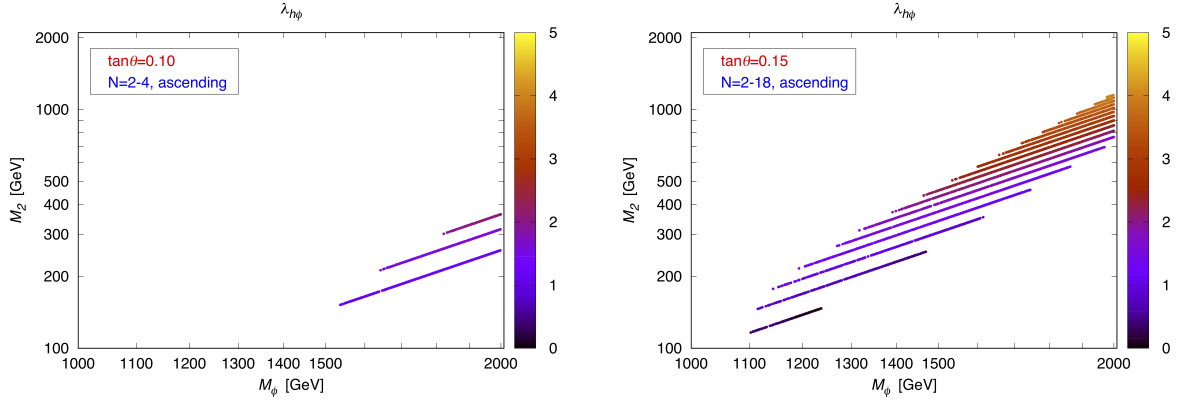


FIG. 7. Solution points satisfying both relic density and direct detection constraints for various values of N . There are no allowed parameter sets for $t_\theta \leq 0.05$.

since the more we have the DM species, the smaller those portion to the relic density should be, which means the larger annihilation cross section of one species of the DM. This effect is demonstrated with the aid of color contours in Fig. 7. We also find that there are no allowed parameter sets for $t_\theta \leq 0.05$. If we increase the mixing angle, more allowed points are obtained but the mixing angle cannot be too large. For example, there are no allowed points for $N = 2$ when $t_\theta = 0.2$ with the DM mass up to 2 TeV.

A few comments on other experimental constraints are in order. There are observational constraints on DM annihilation cross section such as Fermi-LAT [84] and H.E.S.S. [85] measurements. They give stringent limits on the annihilation cross sections of the DM, especially on $b\bar{b}$ and $\tau\bar{\tau}$. But those constraints grow stronger for a lighter DM mass, around less than 800 GeV, while our model prefers DM mass heavier than about 1 TeV. Furthermore, in the high mass region, our model predicts far smaller cross sections than the experimental constraints. More recently, Profumo *et al.* [93] suggested that the annihilation cross section of the DM to a mediator pair can be constrained by considering their successive decays to SM particles. They showed that the upper bound of the annihilation cross sections must be $\sigma v_{\text{DM}} \sim 10^{-25} \text{cm}^3/\text{s}$ for the DM mass around 1 TeV. In our model, the DM annihilation to an h_1 pair was considered and its value lies around $\sim 10^{-26} \text{cm}^3/\text{s}$ which is well below their bound when multiplied by the branching fractions of the SM-like Higgs boson to SM particles, of which values is smaller than a few percent. Since there is an extra scalar mediator in our model, we should also consider the observational constraint to the extra scalar particle. Big Bang Nucleosynthesis (BBN) gives a constraint on the lifetime of the extra scalar particle h_2 less than 1 second [86, 87], and it is well satisfied in our model. There are also constraints from the collider experiments. Our

choice of the mixing angle $t_\theta \leq 0.2$ is quite safe against the LEP2 constraints since the h_2 mass is below around 300 GeV for the DM mass up to 2 TeV. Non-observation of Higgs-like particles in the high-mass Higgs searches through WW and ZZ modes [88–90] at the LHC also provides additional constraints under which our model still survives. There are also constraints on the mixing angle from the signal strength measurements by ATLAS [91] and CMS [92] collaborations, but they do not give severe restrictions to our analysis either.

V. SUMMARY AND CONCLUSION

In summary, we studied a classically scale-invariant DM model of scalar dark matters. The model extends the Higgs sector to have an additional electroweak singlet scalar mediator, scalon, together with a scalar multiplet of global $O(N)$ symmetry, and the electroweak symmetry is broken via the CW mechanism. The scalon serves as the pseudo NambuGoldstone boson of scale symmetry breaking, and the scalar multiplet ϕ can be the viable DM candidate. The DM scalar ϕ couples directly to the SM Higgs with the coupling $\lambda_{h\phi}$ which plays an important role in DM phenomenology.

With the most general conformally invariant Lagrangian, we employed the framework of GW, where a flat direction at tree level is lifted by radiative corrections. Through the mixing of the scalon with the SM-like Higgs boson, two light scalar particles h_1 and h_2 emerge in the model that interact with both visible and hidden sectors. After EWSB, the SM Higgs h_1 and the DM scalars ϕ have the tree-level masses while the new scalar singlet h_2 acquires its mass through radiative corrections of the SM particles and ϕ as obtained in Eq. (13), so that h_2 mass M_2 is dependent on the scalar mixing angle θ and the DM mass M_ϕ .

With three independent new parameters t_θ , M_ϕ , and $\lambda_{h\phi}$, we presented the allowed region of NP parameters satisfying the recent measurement of the relic abundance in Fig. 3 for $N = 2$ case. We also showed the spin-independent DM-nucleon scattering cross section of the scalar DM by varying the DM mass M_ϕ with parameter sets allowed by the relic density observation, and compare the results with the observed upper limits from various experiments in Fig. 5. In the figures, one can clearly see that the allowed parameter space constrained by the relic density observation are located in the mass region of M_ϕ heavier than about 1 TeV. We performed the numerical analysis for $\theta \leq 0.2$, and the $t_\theta \leq 0.05$ case is disfavored in this model due to the recent Xenon1T bound. For $N > 2$, we showed in Fig. 7 that having a too large value of N is disfavored especially due to the direct detection bounds. We also found that our model is not constrained by the current indirect detection bounds for the given parameter sets.

This model can be expanded by introducing complex scalars and/or a gauge symmetry in the hidden sector as well if necessary. Furthermore, our model can possibly resolve the unexplained anomalies in the CMB, so-called the small-scale problems in galaxy formation, due to the existence of the DM self coupling λ_ϕ , and it will be given in our forthcoming studies.

ACKNOWLEDGMENTS

This work was supported by Basic Science Research Program through the National Research Foundation of Korea (NRF) funded by the Ministry of Science, ICT, and Future Planning under the Grant No. NRF-2017R1E1A1A01074699, and funded by the Ministry of Education under the Grant Nos. NRF-2016R1A6A3A11932830 (S.-h. Nam) and NRF-2018R1D1A1B07047812 (D.-W. Jung).

-
- [1] G. Aad *et al.* [ATLAS Collaboration], Phys. Lett. B **716**, 1 (2012).
 - [2] S. Chatrchyan *et al.* [CMS Collaboration], Phys. Lett. B **716**, 30 (2012).
 - [3] W. A. Bardeen, FERMILAB-CONF-95-391-T, C95-08-27.3.
 - [4] T. Hur, D. W. Jung, P. Ko and J. Y. Lee, Phys. Lett. B **696**, 262 (2011).
 - [5] P. Ko, Int. J. Mod. Phys. A **23**, 3348 (2008).
 - [6] P. Ko, AIP Conf. Proc. **1178**, 37 (2009).
 - [7] P. Ko, PoS ICHEP **2010**, 436 (2010).
 - [8] T. Hur and P. Ko, Phys. Rev. Lett. **106**, 141802 (2011).
 - [9] M. Heikinheimo, A. Racioppi, M. Raidal, C. Spethmann and K. Tuominen, Mod. Phys. Lett. A **29**, 1450077 (2014).
 - [10] M. Heikinheimo, A. Racioppi, M. Raidal, C. Spethmann and K. Tuominen, Nucl. Phys. B **876**, 201 (2013).
 - [11] M. Holthausen, J. Kubo, K. S. Lim and M. Lindner, JHEP **1312**, 076 (2013).
 - [12] D. W. Jung and P. Ko, Phys. Lett. B **732**, 364 (2014).
 - [13] A. Salvio and A. Strumia, JHEP **1406**, 080 (2014).

- [14] J. Kubo, K. S. Lim and M. Lindner, Phys. Rev. Lett. **113**, 091604 (2014).
- [15] J. Kubo, K. S. Lim and M. Lindner, JHEP **1409**, 016 (2014).
- [16] P. Schwaller, Phys. Rev. Lett. **115**, no. 18, 181101 (2015).
- [17] Y. Ametani, M. Aoki, H. Goto and J. Kubo, Phys. Rev. D **91**, no. 11, 115007 (2015).
- [18] J. Kubo and M. Yamada, PTEP **2015**, no. 9, 093B01 (2015).
- [19] N. Haba, H. Ishida, N. Kitazawa and Y. Yamaguchi, Phys. Lett. B **755**, 439 (2016).
- [20] H. Hatanaka, D. W. Jung and P. Ko, JHEP **1608**, 094 (2016).
- [21] J. Kubo and M. Yamada, JCAP **1612**, no. 12, 001 (2016).
- [22] J. Kubo and M. Yamada, JHEP **1810**, 003 (2018).
- [23] K. A. Meissner and H. Nicolai, Phys. Lett. B **648**, 312 (2007).
- [24] R. Foot, A. Kobakhidze and R. R. Volkas, Phys. Lett. B **655**, 156 (2007).
- [25] K. A. Meissner and H. Nicolai, Phys. Lett. B **660**, 260 (2008).
- [26] T. Hambye and M. H. G. Tytgat, Phys. Lett. B **659**, 651 (2008).
- [27] R. Foot, A. Kobakhidze, K. L. McDonald and R. R. Volkas, Phys. Rev. D **77**, 035006 (2008).
- [28] S. Iso, N. Okada and Y. Orikasa, Phys. Lett. B **676**, 81 (2009).
- [29] S. Iso, N. Okada and Y. Orikasa, Phys. Rev. D **80**, 115007 (2009).
- [30] M. Holthausen, M. Lindner and M. A. Schmidt, Phys. Rev. D **82**, 055002 (2010).
- [31] L. Alexander-Nunneley and A. Pilaftsis, JHEP **1009**, 021 (2010).
- [32] K. Ishiwata, Phys. Lett. B **710**, 134 (2012).
- [33] J. S. Lee and A. Pilaftsis, Phys. Rev. D **86**, 035004 (2012).
- [34] N. Okada and Y. Orikasa, Phys. Rev. D **85**, 115006 (2012).
- [35] S. Iso and Y. Orikasa, PTEP **2013**, 023B08 (2013).
- [36] T. Gherghetta, B. von Harling, A. D. Medina and M. A. Schmidt, JHEP **1302**, 032 (2013).
- [37] M. Das and S. Mohanty, Int. J. Mod. Phys. A **28**, 1350094 (2013).
- [38] C. D. Carone and R. Ramos, Phys. Rev. D **88**, 055020 (2013).
- [39] V. V. Khoze and G. Ro, JHEP **1310**, 075 (2013).
- [40] A. Farzinnia, H. J. He and J. Ren, Phys. Lett. B **727**, 141 (2013).
- [41] O. Antipin, M. Mojaza and F. Sannino, Phys. Rev. D **89**, no. 8, 085015 (2014).
- [42] M. Hashimoto, S. Iso and Y. Orikasa, Phys. Rev. D **89**, no. 5, 056010 (2014).
- [43] C. T. Hill, Phys. Rev. D **89**, no. 7, 073003 (2014).
- [44] J. Guo and Z. Kang, Nucl. Phys. B **898**, 415 (2015).
- [45] S. Benic and B. Radovic, Phys. Lett. B **732**, 91 (2014).
- [46] M. Y. Binjonaid and S. F. King, Phys. Rev. D **90**, 055020 (2014); *ibid.* **90**, 079903 (2014).
- [47] K. Allison, C. T. Hill and G. G. Ross, Phys. Lett. B **738**, 191 (2014).
- [48] A. Farzinnia and J. Ren, Phys. Rev. D **90**, no. 1, 015019 (2014).
- [49] G. M. Pelaggi, Nucl. Phys. B **893**, 443 (2015).
- [50] A. Farzinnia and J. Ren, Phys. Rev. D **90**, no. 7, 075012 (2014).
- [51] R. Foot, A. Kobakhidze and A. Spencer-Smith, Phys. Lett. B **747**, 169 (2015).
- [52] S. Benic and B. Radovic, JHEP **1501**, 143 (2015).
- [53] J. Guo, Z. Kang, P. Ko and Y. Orikasa, Phys. Rev. D **91**, no. 11, 115017 (2015).
- [54] S. Oda, N. Okada and D. s. Takahashi, Phys. Rev. D **92**, no. 1, 015026 (2015).
- [55] K. Fuyuto and E. Senaha, Phys. Lett. B **747**, 152 (2015).
- [56] K. Endo and Y. Sumino, JHEP **1505**, 030 (2015).
- [57] K. Endo and K. Ishiwata, Phys. Lett. B **749**, 583 (2015).
- [58] A. D. Plascencia, JHEP **1509**, 026 (2015).
- [59] K. Hashino, S. Kanemura and Y. Orikasa, Phys. Lett. B **752**, 217 (2016).
- [60] A. Karam and K. Tamvakis, Phys. Rev. D **92**, no. 7, 075010 (2015).
- [61] A. Ahriche, K. L. McDonald and S. Nasri, JHEP **1602**, 038 (2016).
- [62] Z. W. Wang, T. G. Steele, T. Hanif and R. B. Mann, JHEP **1608**, 065 (2016).
- [63] N. Haba, H. Ishida, R. Takahashi and Y. Yamaguchi, JHEP **1602**, 058 (2016).
- [64] K. Ghorbani and H. Ghorbani, JHEP **1604**, 024 (2016).
- [65] A. J. Helmboldt, P. Humbert, M. Lindner and J. Smirnov, JHEP **1707**, 113 (2017).
- [66] R. Jinno and M. Takimoto, Phys. Rev. D **95**, no. 1, 015020 (2017).
- [67] A. Ahriche, K. L. McDonald and S. Nasri, JHEP **1606**, 182 (2016).
- [68] A. Ahriche, A. Manning, K. L. McDonald and S. Nasri, Phys. Rev. D **94**, no. 5, 053005 (2016).
- [69] A. Das, S. Oda, N. Okada and D. s. Takahashi, Phys. Rev. D **93**, no. 11, 115038 (2016).
- [70] V. V. Khoze and A. D. Plascencia, JHEP **1611**, 025 (2016).
- [71] A. Karam and K. Tamvakis, Phys. Rev. D **94**, no. 5, 055004 (2016).
- [72] S. Oda, N. Okada and D. s. Takahashi, Phys. Rev. D **96**, no. 9, 095032 (2017).
- [73] P. H. Ghorbani, Phys. Rev. D **98**, no. 11, 115016 (2018).
- [74] S. Yaser Ayazi and A. Mohamadnejad, JHEP **1903**, 181 (2019).
- [75] S. R. Coleman and E. J. Weinberg, Phys. Rev. D **7**, 1888 (1973).
- [76] E. Gildener and S. Weinberg, Phys. Rev. D **13**, 3333 (1976).
- [77] M. Pospelov, A. Ritz and M. B. Voloshin, Phys. Lett. B **662**, 53 (2008).

- [78] M. Tanabashi *et al.* [Particle Data Group], Phys. Rev. D **98**, no. 3, 030001 (2018).
- [79] A. Belyaev, N. D. Christensen and A. Pukhov, Comput. Phys. Commun. **184**, 1729 (2013).
- [80] G. Blanger, F. Boudjema, A. Goudelis, A. Pukhov and B. Zaldivar, Comput. Phys. Commun. **231**, 173 (2018).
- [81] E. Aprile *et al.* [XENON Collaboration], Phys. Rev. Lett. **121**, no. 11, 111302 (2018).
- [82] D. S. Akerib *et al.* [LUX Collaboration], Phys. Rev. Lett. **118**, no. 2, 021303 (2017).
- [83] X. Cui *et al.* [PandaX-II Collaboration], Phys. Rev. Lett. **119**, no. 18, 181302 (2017).
- [84] M. Ackermann *et al.* [Fermi-LAT Collaboration], Phys. Rev. Lett. **115**, no. 23, 231301 (2015).
- [85] H. Abdallah *et al.* [H.E.S.S. Collaboration], Phys. Rev. Lett. **117**, no. 11, 111301 (2016).
- [86] K. Jedamzik and M. Pospelov, New J. Phys. **11**, 105028 (2009).
- [87] M. Kaplinghat, S. Tulin and H. B. Yu, Phys. Rev. D **89**, no. 3, 035009 (2014).
- [88] O. Gonzalez Lopez, Nucl. Part. Phys. Proc. **273-275**, 907 (2016).
- [89] CMS Collaboration [CMS Collaboration], CMS-PAS-HIG-16-033.
- [90] S. Angelidakis [ATLAS Collaboration], Nucl. Part. Phys. Proc. **282-284**, 199 (2017).
- [91] The ATLAS collaboration [ATLAS Collaboration], ATLAS-CONF-2019-005.
- [92] CMS Collaboration [CMS Collaboration], CMS-PAS-HIG-17-031.
- [93] S. Profumo, F. S. Queiroz, J. Silk and C. Siqueira, JCAP **1803**, no. 03, 010 (2018).